

WIYN Tip-Tilt Module Performance

C. F. Claver^a, C. Corson^b, R. Gomez^a, P. Daly^a, D. Dryden^a, B. Abareshi^a

^aNational Optical Astronomy Observatory; ^bWisconsin-Yale-Indiana-NOAO Observatory

ABSTRACT

The WIYN Tip-Tilt Module (WTTM) is an addition to the existing Instrument Adapter System (IAS) providing a high performance optical-NIR image stabilized port on the WIYN 3.5m telescope. The WTTM optical system uses a 3-mirror off-axis design along with a high bandwidth tilt mirror. The WTTM is a reimaging system with 15% magnification producing a 4x4 arcminute field of view and near diffraction limited imagery from 400-2000nm. The optics are diamond turned in electroless Nickel over an Aluminum substrate. The WTTM opto-mechanical assembly was designed and built using the principals of the "build-to-print" technique, where the entire system is fabricated and assembled to tolerance with no adjustments. A unique high performance error sensor, using an internal mirrorlette array that feeds 4 fiber coupled avalanche photodiode photon counters, provides the tilt signal. The system runs under the Real-Time Linux operating system providing a maximum closed loop rate of 3khz. In this paper we report on the successful lab testing, verification of the "build-to-print" technique and on telescope performance of the WTTM.

1. INTRODUCTION

The performance of an astronomical telescope can be gauged by its aperture, image quality and overall efficiency of observation. We can express this metric as

$$M = \frac{\varepsilon A \Omega}{d\theta^2},$$

where ε is the observing efficiency and includes throughput of the telescope, percentage of time actually used for observations, A is the telescope aperture, Ω is field of view and $d\theta$ is the FWHM of the delivered PSF. Therefore, any measure to reduce the image size results in significant gains in the capabilities of a given telescope.

One of the principal components that degrade the intrinsic image quality of a telescope is image motion, or wavefront tilt. Image motion can come from a variety of sources that can be categorized into three basic properties: 1) Common Mode – this includes sources of physical movement of the telescope facility itself from drive errors, wind bounce, vibrations from fans and other sources. 2) Near Field – these include seeing effects near the telescope pupil such as mirror and dome seeing and low altitude boundary layers. 3) Far Field – these are the high altitude turbulent layers typically modeled when considering atmospheric effects on seeing. In the end, it is the sum total of all of these three types of distortions that contribute to observed image motion at the focal surface of the astronomical telescope.

An extensive period of study from 1995-1998 at the WIYN telescope showed that we could expect 0.1-0.25" in improvement to the FWHM from tip-tilt correction (Claver *et al.* 1998). The median seeing at WIYN is approximately 0.7" FWHM, hence the enhancement of our performance metric from tip-tilt correction would be as high as a factor of 2. According to Tonry *et al.* (1997) at the median WIYN seeing we can expect the 1-axis FWHM of image motion from Kolmogorov turbulence to be 0.44". Subtracting in quadrature from 0.7" we would expect a tip-tilt corrected FWHM of 0.54", or an improvement of 0.16". This is consistent with what Claver *et al.*'s empirical study showed, but also indicates that often there is a considerable amount of image motion from sources other than atmospheric turbulence. Irregardless of its source, reduction of image motion will significantly increase the performance of the WIYN facility.

2. THE WTTM SYSTEM DESIGN

The WIYN telescope is a 3.5m Ritchey-Cretien design with an f/1.75 borosilicate spun cast primary mirror from the University of Arizona Mirror Lab. The secondary mirror with a magnification of 3.59 produces the final f/6.39 focal surface. The final beam is directed by a tertiary to either of two Naysmith ports, one holding the wide field Hydra multi-object spectrometer and the other hold the Instrument Adapter System (IAS). The IAS is used for direct imaging

programs and supports wavefront measurement, guiding, calibration lamps, interfacing to the Filter-Shutter Assembly (FSA) and the CCD dewar. Additionally the tertiary can be removed from the optical path to allow a Cassegrain focus with an $f/13$ reimaging system. This configuration allows the WIYN telescope to access any one of these primary instrument ports quickly over the observing night, thus providing a maximum of flexibility for science programs.

The WIYN Tip-Tilt Module (WTTM) is designed as an extension to the WIYN IAS to add an additional imaging port with fast tip-tilt compensation. The design was driven by the need to quickly change, in $< 5-10$ minutes, between the WTTM and the extant wide field imaging port supported by the IAS. In addition we aimed to maintain system image quality of $\leq 0.3''$, as not to compromise the imaging performance of the telescope itself. Figure 1 shows the newly reconfigured IAS with both imaging ports side-by-side.

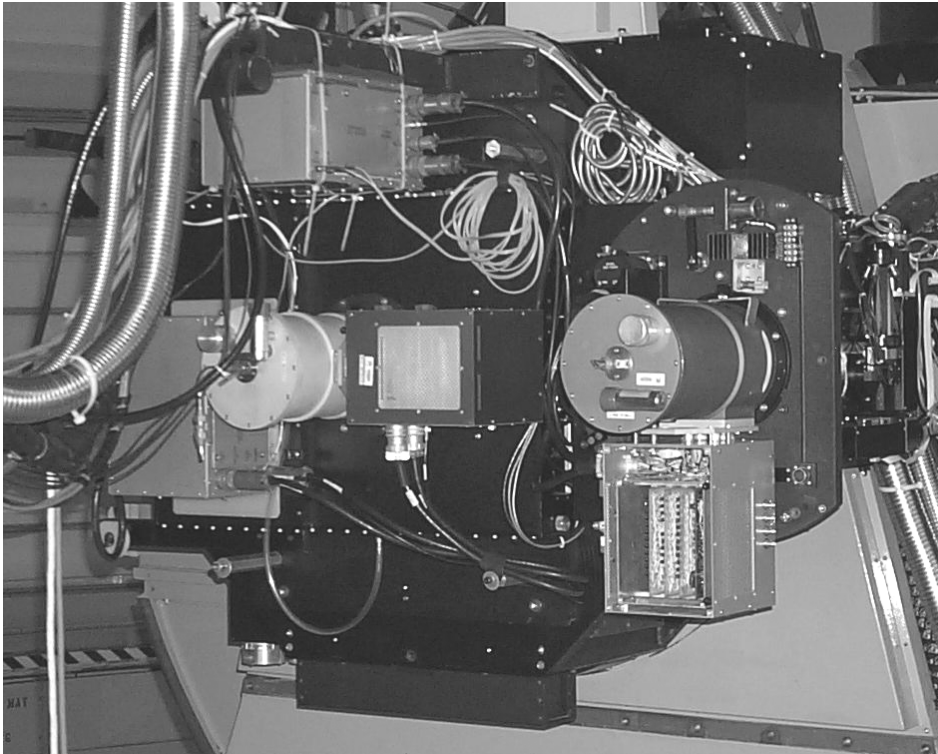


Figure 1: The WIYN IAS with both the 10 arcminute FOV Mini Mosaic (Left) and the tilt corrected 4 arcminute FOV WTTM (right).

2.1 Optical System

Because of space constraints and the demand to quickly switch from wide field uncompensated imaging and tilt compensation we chose a folded re-imaging design that is closest to a modified Offner relay (see Fig. 2). In this design we use a single spherical mirror (M1) to image the pupil on the flat tip-tilt mirror followed by a 2-element off-axis reflective camera using a convex asphere (M2) and concave sphere (M3) to re-image the field. Following the camera the light is diverted between the science and error sensor branches by a flat beam splitter, where the front surface reflection is toward the science camera. The WTTM optical system has a magnification of 1.33 that results in a final plate scale of $7.66''/\text{mm}$ at $f/7.45$, so that it samples well the best of the expected delivered images, over a 4 arcminute field of view.

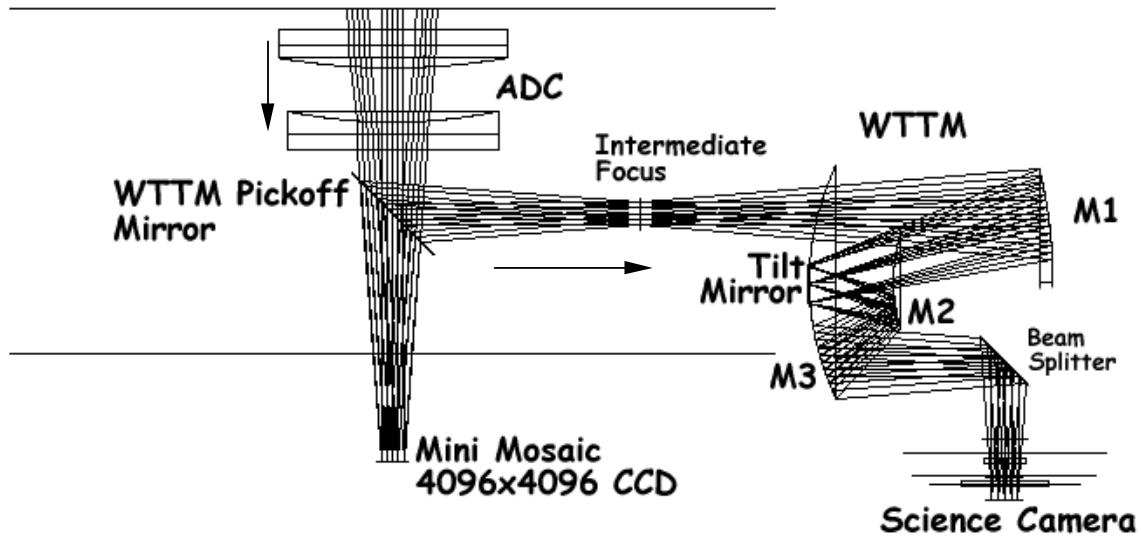


Figure 2: The light path inside of the WIYN IAS showing for both the Mini Mosaic and WTTM that are selected with the movable pickoff mirror.

2.2 Opto-Mechanical Design

The optical housing of the WTTM is constructed of three principal cells, each holding one of the three off-axis mirrors. In our realization of this design we adopted the “build to print” philosophy. Simply put, “build-to-print” means that there are *no* adjustments in the opto-mechanical system, in which each part or subassembly is toleranced to meet specifications and is built to print. There were two principal drivers for choosing this approach: 1) Due to the off-axis optical design there was no deterministic solution to alignment based on optical feedback that would ensure us meeting our imaging performance goals. 2) From a management perspective, if executed properly, this philosophy would greatly accelerate the assembly, testing and commissioning phase of the project.

Once we settled on our mechanical design we implemented the “build-to-print” process starting with fabrication of the least deterministic part of the system, the optics. Critical to realizing our design performance was having reference surfaces on the optical elements that could be traced directly to the final optical surface. Each of the off-axis optical elements in the WTTM has three axial pads and a radial boss that are directly related to the optical surface. It is these surfaces that are used to define the location of each element in their respective cells.

The off-axis optical elements were fabricated in nickel plated aluminum substrates by a multi-step diamond turning process. Each of the three mirrors were fabricated as pairs in a four piece assembly consisting of the mirror pairs, a surround and base-plate. In this assembly the mirror pairs were situated opposing each other, the surround filled the area around the mirrors to synthesize an axial symmetric piece and the base plate served as our reference for axial positioning. As part of the process the radial boss was diamond turned during the same setup as the optical surface, thereby making it directly tied to the optical axis of the parent surface. The precise diameter was measured and recorded for matching these to locating pads in the individual cells. Once the final surface was turned in the nickel the central thickness was measured between the parent vertex and the base plate, providing the reference measurement between the axial pads and optical surface. These surfaces by way of their fabrication are tied to the actual optical surface to better than 0.000050 inches and have been verified using precision electronic gauges and ultra precise air bearing table.

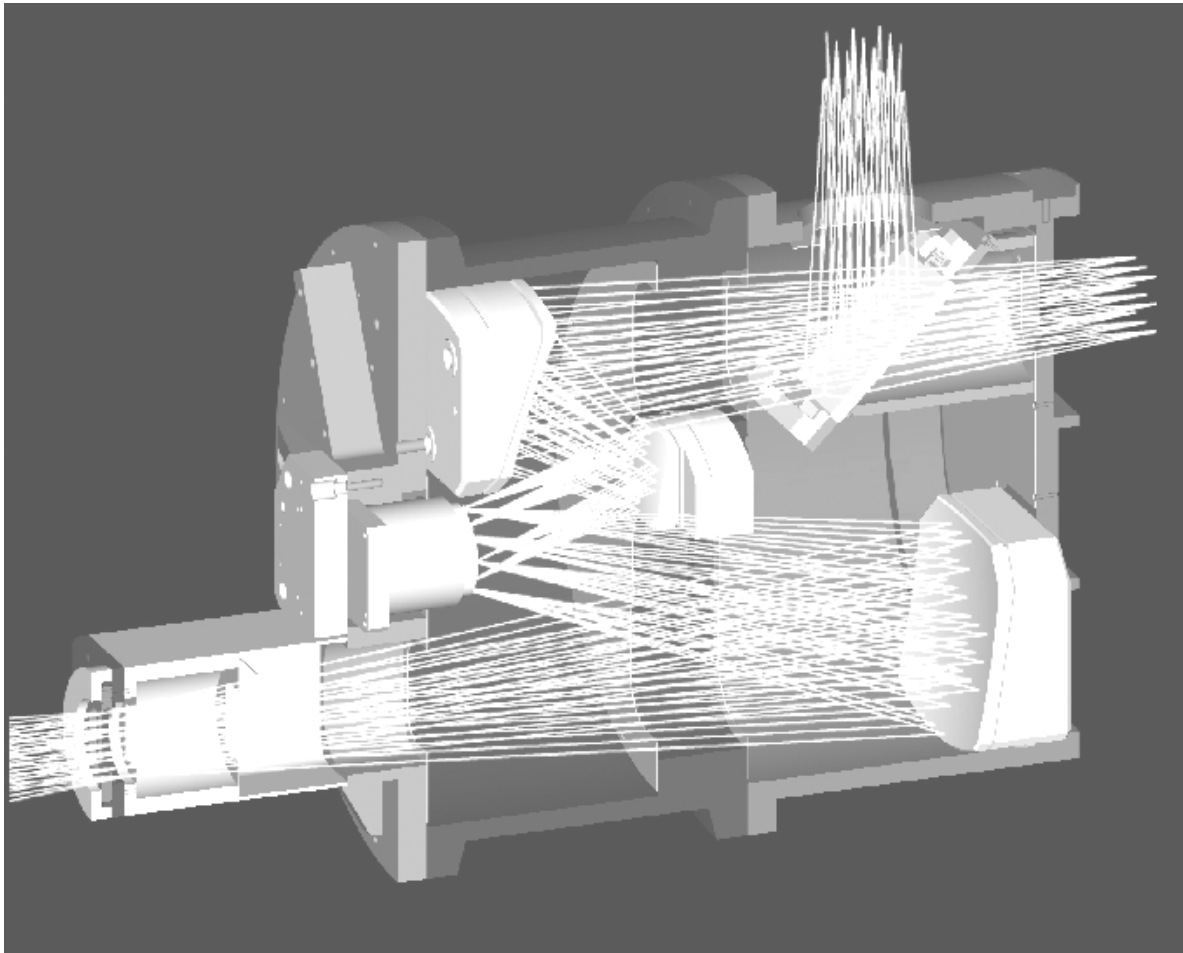


Figure 3: A cutaway view of the WTTM optical housing. Note the lack of adjustment at the optical mounting points.

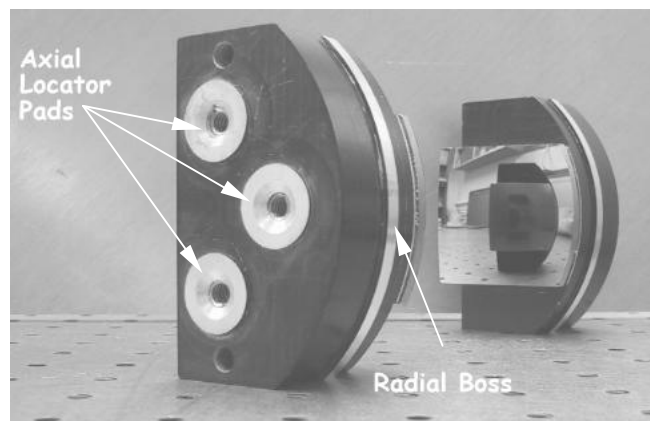


Figure 4: M2 showing the location of the axial pads and radial boss used for precision locating the optical surface.

With the measurements of the physical reference surfaces along with the as-built radius of curvature for each of the optical surfaces we balanced the optical design to optimize the imaging performance. We constrained the optical balancing to only those dimensions that could be affected in the machining process of the individual cells. These cells we rough machined during the optical fabrication leaving enough material in critical locations to accommodate the final

balanced dimensions. This ability to balance the optical design just prior to the final dimensioning of the critical components is essential in making the “build-to-print” approach work. Further, it is equally important to qualify that each component meets its dimensional specifications with independent measurement, apart from the fabrication process.

2.3 The Tip-Tilt Error Sensor and Active Components

The error sensor in the WTTM (Figure 3) is a unique design using an internal mirrorlette array to dissect the image of the guide star into quadrants. The first element in the error sensor is the compensator. This element corrects much of the astigmatism introduced by the beam splitter as the light passes through it. In addition the compensator corrects for chromatic aberration in the error sensor optical system. Following the compensator an aperture wheel is used to select between one of six circular field stops, the full field of the error sensor is 4 arcseconds. The light is then re-imaged with a magnification of approximately 140 onto the mirrorlette array. The mirrorlette array focuses an 80 μ m pupil image in to the optical fiber, which feeds one of four EG&G (now Perkin-Elmer) SPCM-AQR-14 avalanche photo-diode modules.

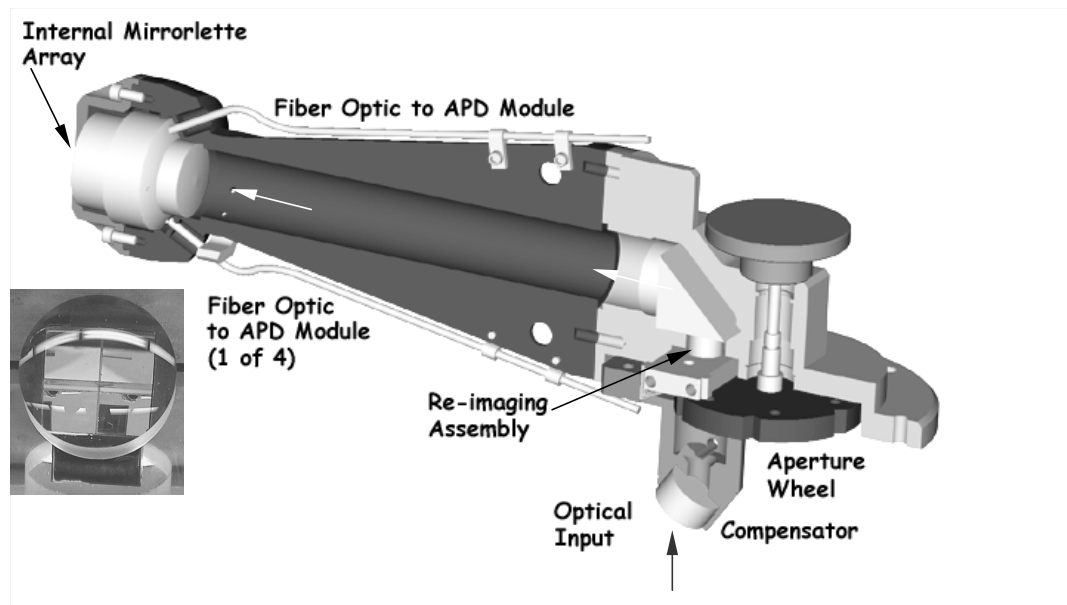


Figure 5: A cross-sectional view of the WTTM error sensor. The inset shows the mirrorlette array during fabrication in the NOAO optical shop.

Because of its thickness (~10mm) the beam splitter introduces a significant amount of aberration to the error sensor optical beam. By far the dominant aberration is astigmatism. The compensator corrects much of this, but we leave some remaining and use the optical properties of astigmatism to sense focus with the quadrant detector, described in detail by Vaughn *et al.* (2000). The error sensor sub-assembly moves on a high precision X-Y stage used to position the error sensor on the user selected guide star.

The closed loop tilt correction is accomplished by a Physik Instrumente S-340 tilt platform driven with their high power 200W amplifiers. These amplifiers with the S-230's 7.2 μ F capacitance on each axis yield a bandwidth of >500Hz at 50% of the maximum amplitude and >2000Hz at 10% amplitude. We found the tip-tilt stage with the mirror attached to have natural resonances of approximately 800Hz in both axes.

2.4 Computer System

The computer system used to run the WTTM is based on a dual 500Mhz dual CPU Pentium computer running Real-Time Linux (Daly *et al.* 2000). The computer holds the counters used to measure the photon pulses from the SPCM

modules, digital-to-analog converters to the Physik Instrumente chassis and interfacing to the rest of the WTTM hardware. The error sensor positioning stage is controlled from the computer over an RS232 serial line to a separate control chassis for the X-Y stage. The user controlled functions specific to the WTTM are handled by this computer through a set of Graphical User Interfaces (GUI). These include, frequency selection of the closed loop, gain selection and positioning of the error sensor.

3. LAB TESTING AND PERFORMANCE

3.1 Static Optical Testing

The optical performance of the WTTM has proven to be superb. After just one day of assembly in the lab the WTTM optical system was delivering near theoretical performance. By placing a 5x5 grid of 5µm diameter pin holes at the input of the WTTM (the intermediate focal surface) we have evaluated the WTTM optical performance in the absence of any atmospheric distortion. The 5µm diameter pin holes are diffraction limited in this design. Using a video camera fed by a microscope objective we were able to capture high-resolution images of the as built diffraction image (Figure 5). The agreement with the theoretical diffraction images from the Zemax raytrace software is excellent.

A more quantitative measure of the imaging performance was done using our science imaging system to image the entire 5x5 pin hole grid. The science imaging system uses an EEV-80, which has 13.5µm pixels. We extracted sub-rasters around each pinhole image, registered these and then combined them to form an “average” PSF image for the full FOV. The encircled energy of this average PSF is shown in the right panel of Figure 5 along with the theoretical plot from Zemax.

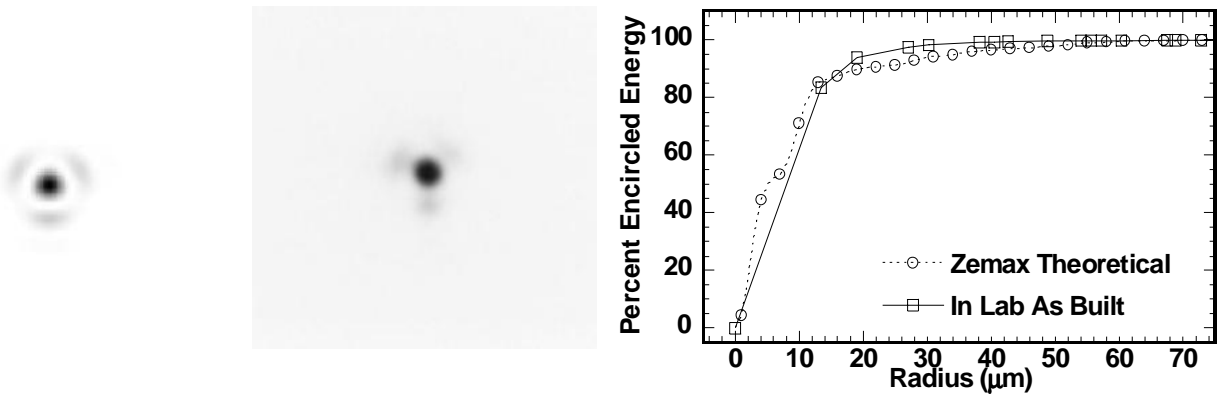


Figure 6: A comparison between the theoretical white light diffraction image as computed from Zemax (left) and the as built diffraction images as recorded by our microscope at the center of the FOV (center). The right panel shows the comparison of theoretical and measure encircled energy.

3.2 Closed Loop Performance

During our lab tests we explored the limits of the closed loop performance. Our first tests aimed at exploring the maximum rate the computer system could measure the 4 photon counters, compute the mirror command voltage and send this to the tip-tilt mirror system. We found that when no other activity was present on the computer that a rate of 10kHz could be achieved. While in practice this rate can never be realized due to the finite mechanical bandwidth of the tip-tilt platform, it does give us a measure of the internal latency in the system. Further tests showed that the 100µsec of latency consists of roughly 10µsec to read the 4 APD counters, 80µsec to send the X-Y tip-tilt mirror position and 10µsec of additional overhead. Minimizing the system latency helps reduce correction errors caused by the evolution of the true wavefront tilt while the system computes and applies the measured tilt.

By examining the step response of the system, we include the physical effects of the tip-tilt mirror including mechanical inertia and drive amplifier limitations. With the WTTM in the lab we used the 5x5 pin-hole grid to close the loop between the error sensor and tip-tilt mirror. The system was configured so that photon rates did not impose a significant limit to the system bandwidth. Once the loop was closed we effectively opened the loop by setting the system gain to zero. The error sensor was then moved by an equivalent of one arcsecond on the sky to insert a step error to the system. The loop was closed by resetting the system gain to a non-zero value and the mirror commands and error signals recorded. The gain value was tuned to maximize the system response with minimal overshoot for each test at increasing loop speeds.

Figure 7 shows an example of the step response at a 3kHz loop frequency. We see a phase delay between the mirror command and the response in the error sensor signal corresponding to approximately 1 msec. Full settling of the system occurs after 3 msec, while 50% of the step is compensated within 2 msec. From these tests we find that the maximum half-power bandwidth of the system is approximately 500Hz.

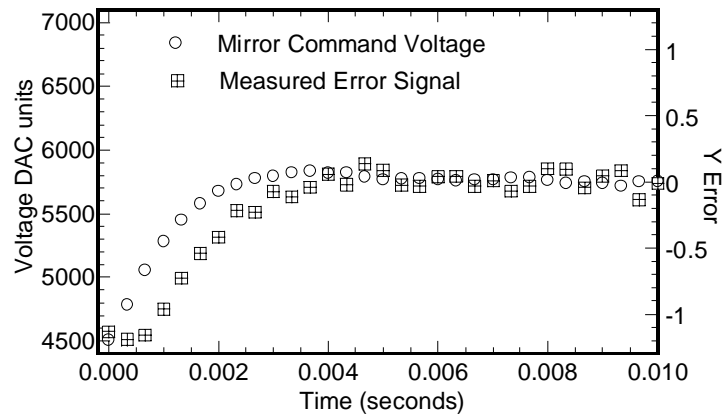


Figure 7: An example of the WTTM system step response function while operating at a loop frequency of 3kHz.

4. ON-SKY TESTING AND PERFORMANCE

The WTTM had its first light run on 23 February 2002. Since then, the WTTM has had several Testing and Engineering nights at the telescope for the purpose of debugging and characterizing its performance. Here, we present some of the preliminary results from this testing period.

For the purpose of commission we used a simple beam splitter using a thin 75Å layer of aluminum on a BK-7 substrate. This results in approximately 60% of the incident beam to be reflected toward the science branch, 20% transmitted to the error sensor branch and 20% loss through absorption. With this configuration we are able to operate the WTTM at 500Hz using a V=15.5 magnitude guide star. This is substantially faster than our design estimates predicted.

The relationship between the error sensor signal and the applied correction on the tip-tilt mirror is controlled by a relative gain for each axis. Under typical operation we choose identical gains for each axis. During several observing runs under a variety of conditions we measured the corrected FWHM of the guide star as a function of this gain setting. We found that there is typically a broad minimum in FWHM implying that the optimum gain setting is relatively insensitive to the specifics of the operating conditions. Figure 8 shows the changes in FWHM through the R filter versus gain during a test where the closed loop rate was operated at 400hz. During these test the closed loop rate was adjusted for a signal-to-noise ratio in the error signal of approximately 5.

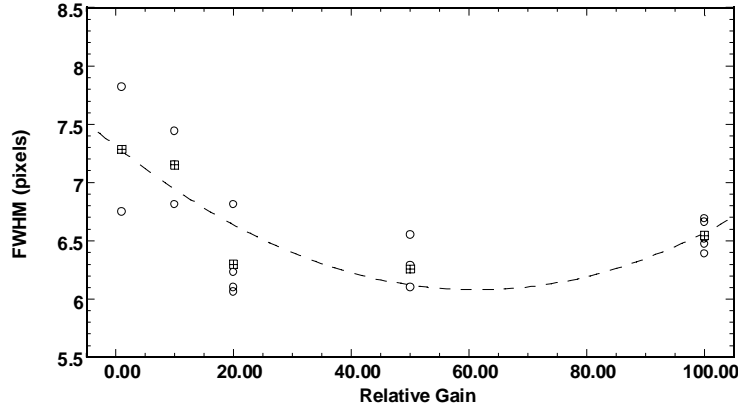


Figure 8: FWHM versus relative gain.

During the first light observing run we obtained correction in the FWHM from 0.71" to 0.53", which resulted in a 50% increase in the central brightness of the PSF. Figure 7 shows the radial profile of corrected and uncorrected PSF from this first light run. In practice we have found that the largest improvement to the delivered image quality with the WTTM comes when the native seeing is between 0.5-0.8". When the seeing is poor, >1.0" FWHM, there is significant image motion corrected by the WTTM, but higher order aberrations appear to dominate the image quality. When native seeing is good, <0.45" FWHM, we see a variety of results in the improvement from tip-tilt correction. In many instances there is very little improvement under these conditions. On rare occasions we have seen exceptional improvement with tilt corrected images of 0.28" FWHM.

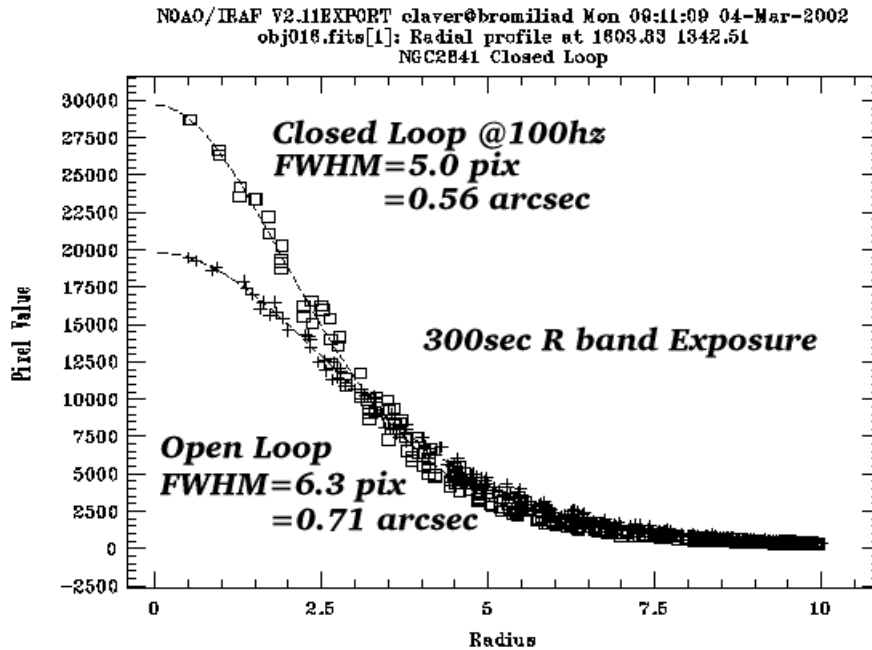


Figure 9: First light radial profiles of the corrected and uncorrected images from the WTTM.

In one test we obtained a series of 10sec. exposures, alternating between closed loop tilt correction and uncorrected exposures, shifting the charge between each exposure to allow 10 exposure pairs to be taken in rapid succession. This allowed us to minimize the effect of changing conditions to confuse the results due to long CCD readout times. We obtained 5 image sets containing a total 50 image pairs. The open loop, uncorrected, images have an average FWHM=4.84 pixels (0.53") \pm 0.33 pixels (0.04"). Under these conditions the closed loop, tilt corrected at 1000Hz, images showed a wide range of improvement, with roughly 30% of the time no improvement was evident. The remaining 70% of the time the average delivered FWHM=4.06 pixels (0.45") \pm 0.21 (0.02").

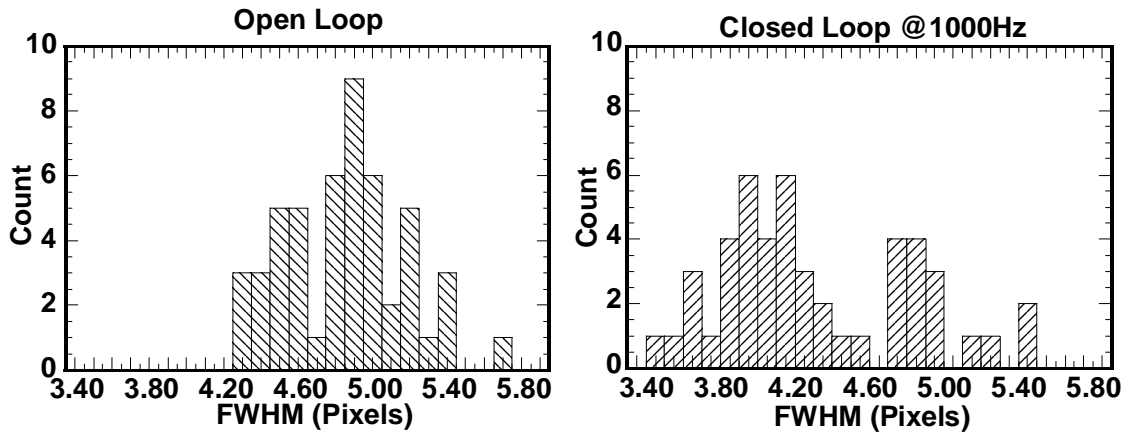


Figure 10: Seeing distributions of tilt corrected images (right) and uncorrected images (left).

In the original image motion study by Claver *et al.* the correlation of image motion was measured to be greater than 90% over a radius of 150 arcseconds. We have found that over the 4 arcminute FOV of the WTTM that PSF variations due to the finite correlation radius are only noticeable in the very best of conditions. Figure 11 Shows the FWHM in good conditions as a function of distance from the star used to determine the tilt correction. This is similar to what Tonry *et al.*(1997) found in their study at the MDM 2.4m telescope. They concluded that the degradation of corrected FWHM was faster than that predicted by Hufnagel-Valley atmospheric turbulence profile and was caused by the actual turbulence at a lower altitude. This similarity is not surprising because both WIYN and the MDM telescope share similar site with respect to the prevailing wind direction and the location on the Southwest Ridge of Kitt Peak, AZ.

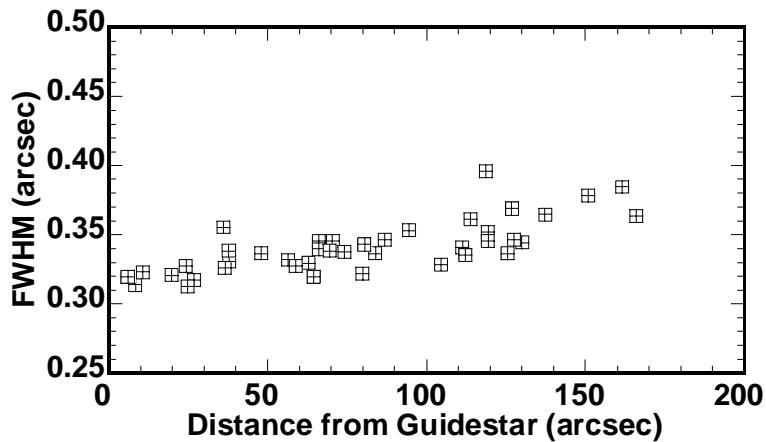


Figure 11: The FWHM of the tilt corrected images from the WTTM as a function radial distance from the guide star.

4.1 Preliminary results from the DALSA high speed CCD camera

During the last of the engineering runs with the WTTM prior to the Arizona summer rains we were able to test a new high speed DALSA CCD camera system. We aimed to use the camera in place of the science CCD system to characterize the power spectra of the WTTM image motion under a variety of conditions, gains and loop rates. During these first tests we were blessed with very good native seeing of 0.4", hence the power in the uncorrected spectrum is significantly lower than other studies. We obtained the corrected power spectrum while the WTTM was operating at a closed loop rate of 1000hz.

From these data we have learned that the low frequency correction is somewhat poorer than expected for a given correction rate. We are able to improve the low frequency performance by increasing the loop gain, however this results in increased power at high frequencies. We interpret this as a byproduct of the simple proportional loop used to apply the error sensor signal to the tilt mirror. As of this writing we are adding an integral term to the servo loop, which will improve the low frequency performance without over driving. In spite of this shortcoming Figure 12 shows a significant reduction in overall power beyond 100hz when we have the luxury of a bright guide star to operate at 1000hz.

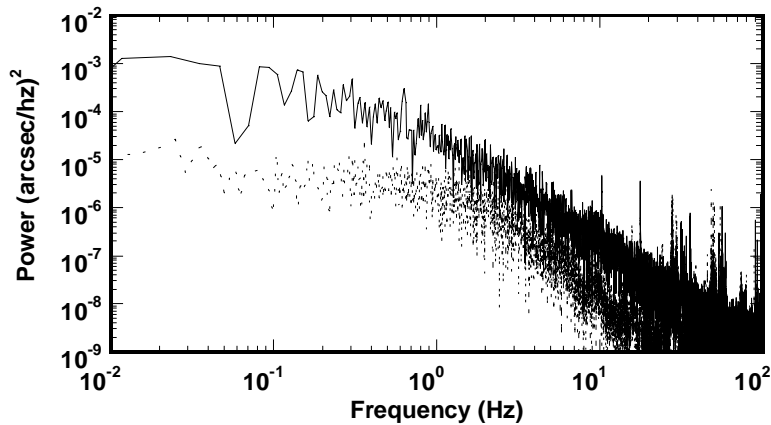


Figure 12: The power spectrum of 1-D image motion at WIYN during our early DALSA high-speed camera study with the WTTM, with uncorrected power (solid line) shown with the corrected power spectrum (dashed line)

5. CONCLUSIONS

We have presented a brief look at preliminary characterization of the WIYN Tip-Tilt Module that adds real-time tilt correction to the WIYN facility. In our lab testing we have found the hardware and electronics perform at a level that does not limit the performance of the WTTM on the sky. In normal use the performance of the WTTM to correct image motion should be limited only by the signal-to-noise ratio of the error signal. Further, the intrinsic image quality of the WTTM is essentially identical to the theoretical design. The closed loop performance shows significant gains in most instances to the delivered image quality and will certainly increase the performance metric of the WIYN telescope. A more thorough treatment of the performance of the WTTM will come as we gain more experience with this new instrument.

6. REFERENCES

- Claver, C. F., Jacoby, G., Silva, D. and Code, A. D., 1997, SPIE Proc., 3353, 1130
- Daly, P. N. and Claver, C. F., SPIE Proc., 2000, 4009, 71
- Vaughnn, D., Claver C. F. and Richardson, E. H., 2000, SPIE Proc., 4008, 1413
- Tonry, J. L., Burke, B. E. and Schechter, P. L., 1997, PASP, 109, 1154